OPTICAL STUDIES

The detailed optical investigations aimed at the identification and dimensional characterization of a statistically significant number of tracks and pits, including structures < 3 mm long. We purposefully excluded the flake and/or droplet impacts from these investigations, because they are of local, somewhat idiosyncratic provenance related to the disposition of waste products, and because they were well characterized by PPMD and POSA. Their inclusion into the time-consuming optical survey would have slowed down operations considerably, thus distracting from the major objective which was the characterization of high-velocity impactors in

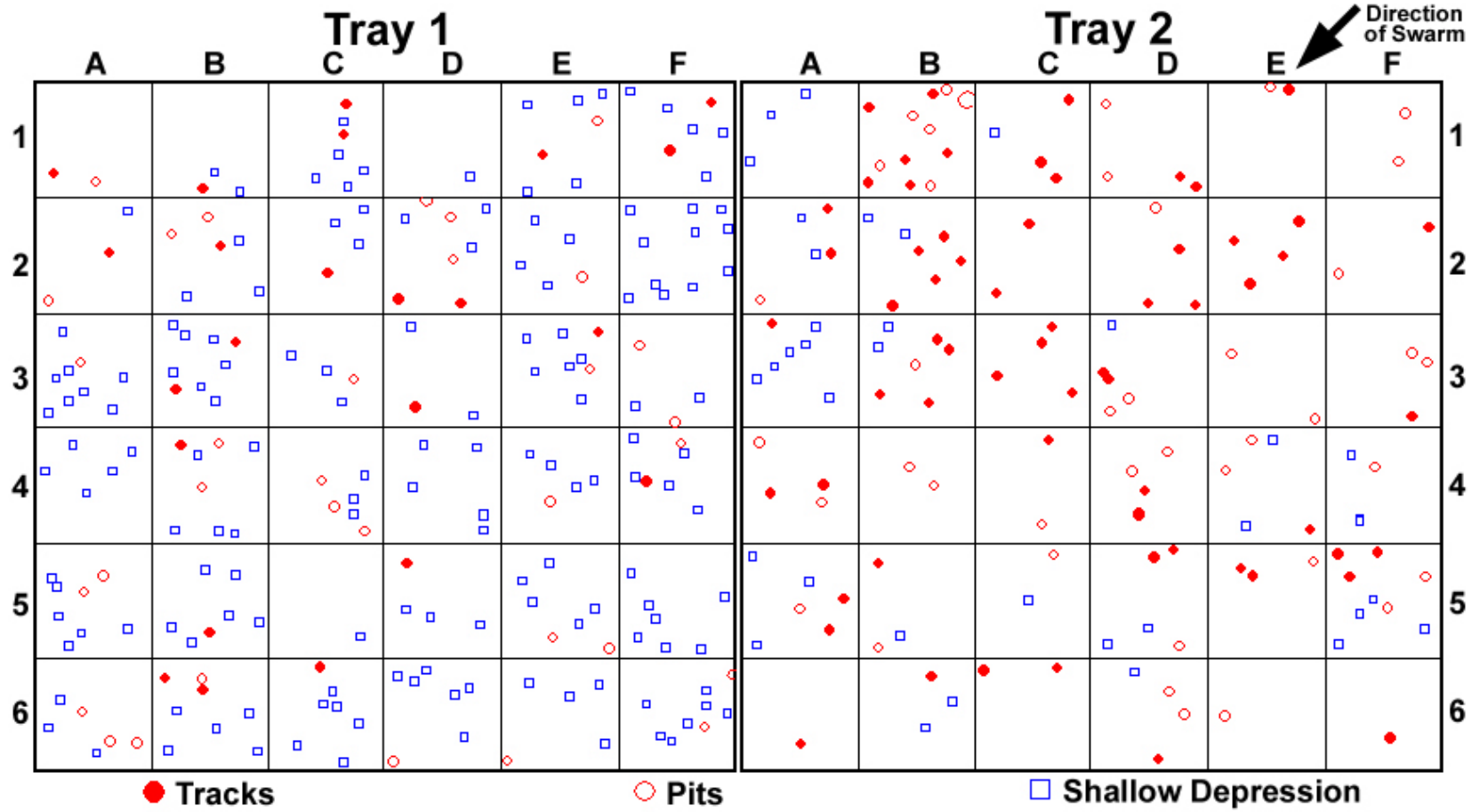

Figure 30. The distribution of impact features > 3 mm classified into three major categories.

LEO. In addition, we did not maintain the distinction between tracks and pits during this portion of our investigation, much less record detailed morphologic subclasses, some of which we only recognized during the course of the microscopic survey and/or SEM investigations. Consequently, we referred to all features as tracks in the microscopic observations and documentation phase.

Procedures

Detailed optical studies of the ODC tiles were conducted in the FOILS laboratory (see Figure 31) that is equipped with a scanning platform, a binocular microscope, and high-resolution digital-imaging system, all interconnected and controllable by computer. In detail, the FOILS system consists of a large scanning platform (*i.e.*, a modified Mann Comparator) that can be translated horizontally along two directions (X and/or Y axes) by remotely controlled stepping motors with a precision of < 2 µm. The sample being analyzed (aerogel tile) resides on the scanning platform, which is driven via computer control past a stationary binocular microscope (Wild M8; equipped with diverse lenses, illumination systems, and a beam splitter which accommodates a Sony DKC 5000 CCD camera). A third stepping motor raises and lowers the entire microscope system for purposes of (a) focusing and (b) the measurement of vertical dimensions (z-axis). The Z-axis is controlled via a rocker switch for focusing the microscope up and down, with individual steps equaling 4.25 µm in distance. The position of all three axes/stepping motors is monitored and continuously displayed on the PC monitor.

Characterization of individual tracks during optical scanning required a minimum of two sets of measurements. The 0,0 corner of each tile is defined as the intersection of the tile edges below and to the left of the silver-paint fiducial mark. Step one involved placing the center of the entrance hole or feature under the crosshair in sharp focus, such that the X/Y coordinates provided for the location in a tile specific reference frame. The Z-axis read-out is then reset to zero (0), as the measurement referred to the local tile surface. The scanning platform is then driven to the terminus of the feature, with the impactor residue - if present - or the deepest point of a pit being brought into sharp focus and centered under the crosshair. A second set of coordinates (*i.e.*, X'/Y'/Z') is recorded. Employing trigonometric relationships, these measurements uniquely define the absolute depth, length, inclination, and azimuthal orientation of each track in a tile-specific reference frame. Additional measurements on select tracks related to residue size or to the diameter of pits were acquired at this time.

The microscope mounted CCD system also interfaced with the computer and provided for convenient viewing at a wide variety of magnifications, as well as for the capturing of digital images. The majority of images in this report were taken by this system. The bluish background of these images is the result of light scattering by the aerogel during front illumination, the latter provided by either a ring-light for even 360° illumination, or by arbitrarily positioned, flexible fiber-optics used to highlight specific details, or both. We also employed traditional, optical (Polaroid) cameras and back-light illumination to highlight specific details of tracks during sample preparation for SEM analyses; this back-lit, black and white photography was especially valuable for the documentation of trapped particles.

The rate-controlling factor in the detailed optical analysis of aerogel is undoubtedly the strain on the microscopist's eyes. The intrinsic surface roughness and transparent nature of aerogel is

Figure 31. View of the optical inspection station consisting of scanning platform, binocular microscope, CCD camera, and interactive PC system of the JSC FOILS laboratory.

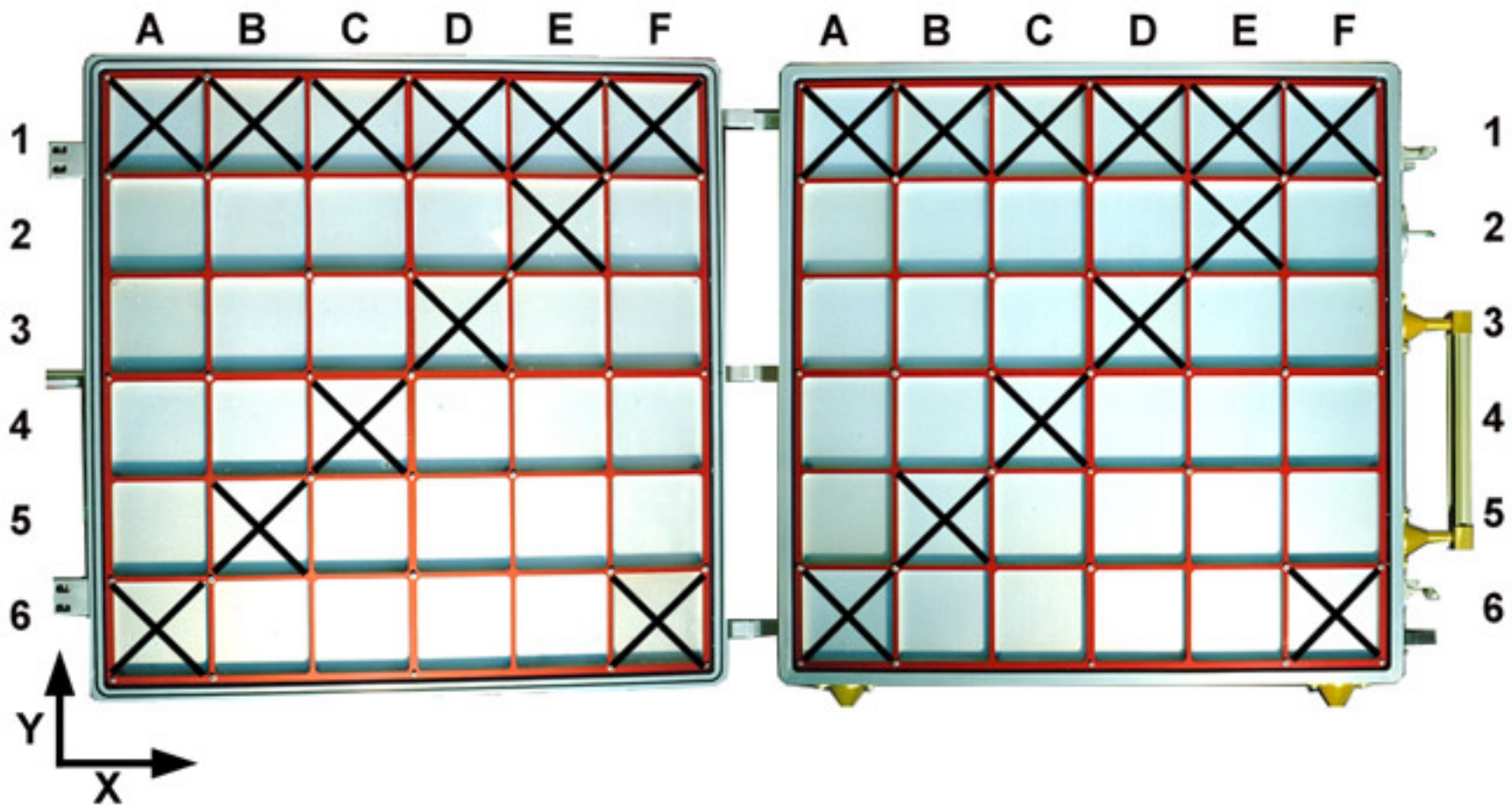

Figure 32. Location of the 24 tiles that have been scanned to date utilizing the FOILS laboratory system.

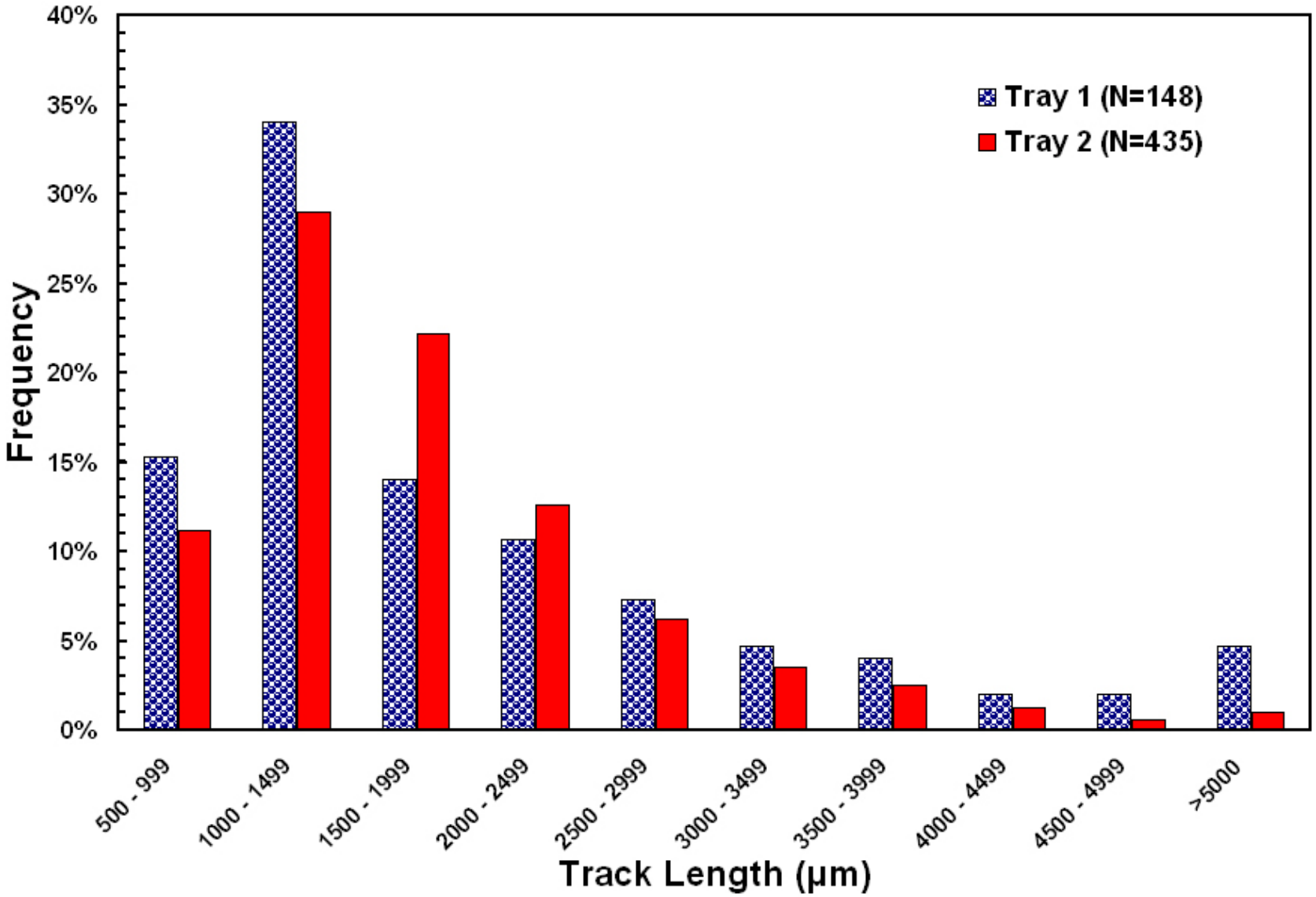

Figure 33. Frequency histogram of absolute track lengths > 0.5 mm encountered on ODC. Note the grossly similar distributions on both trays.

especially taxing, with even the most dedicated individuals not scanning for more than five hours a day, typically split between a morning and an afternoon session. Initially, we set out to record all features > 50 µm in size, mandating an ~ 1 mm wide field-of-view during scanning operations, and resulting in ~ 100 scan passes to cover an entire 10 x 10 cm tile. Each 1 mm wide pass took an hour or more to complete, even for the most experienced observer. This resulted in an unacceptably low rate of progress. Therefore, we raised our minimum dimensions to features > 100 µm. As a result, scan time per tile was reduced to ~ 30 hours, still too slow in view of available resources. Ultimately, we settled for the quantitative recording of impact features > 500 µm in size, which reduced the scan time to ~ 10 hours per tile, or approximately two working days/tile. To date, we have completely scanned a total of 24 tiles.

As illustrated in Figure 32, the selection of these 24 tiles was by some arbitrary, yet systematic, geometric criterion with the intent of obtaining representative observations for each of the two trays. Our plans are to complete detailed scans of at least half of all tiles (*i.e.*, 18/tray). This plan is substantially motivated by the fact that it is impractical to subject every optically observed track, even on half of the tiles, to compositional analysis via SEM-EDS methods. The large number of impact features recorded by the ODC aerogel was unexpected and is a testimony to its outstanding performance as a particle collector. As a consequence, decisions had to be made that balance the resources available to produce a statistically meaningful data set on the size-frequency distribution of tracks, versus the acquisition of compositional information, the latter being the primary objective of ODC.

Track Length

The results of our currently completed optical analyses are tabulated in Appendix B. The distribution of track lengths > 500 µm is summarized in Figure 33. These distributions are remarkably similar for both trays, despite the fact that the Tray 2 data are unquestionably contaminated with swarm tracks. Note that very few features are > 5 mm deep, but the data only refer to 12 tiles per tray, approximately 1/3 of the total surface. The grossly similar track populations on both trays imply highly variable MIR attitudes, combined with the wide angle viewing geometry (~ 180°) of each tray, such that both trays could sample similar segments of the sky. However, Tray 2 has an approximate factor of 2 more tracks than does Tray 1; this is -

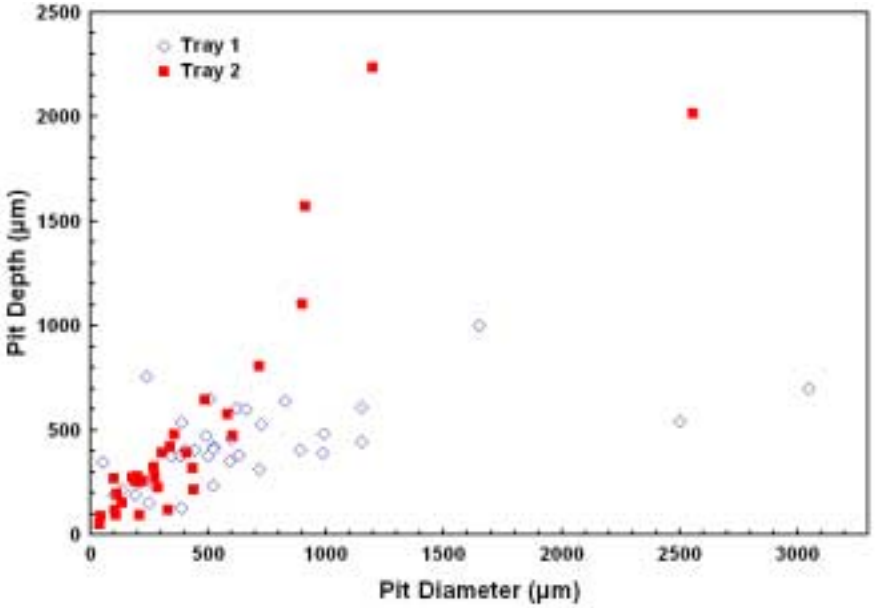

Figure 34. Diameter versus depth relationships of ODC pits, separated into forward (Tray 1) and rearward (Tray 2) facing collector surfaces.

in part - due to contamination with isolated swarm tracks, yet it is possible that Tray 1 was also more shielded than Tray 2.

As previously stated, no distinctions were made between pits and tracks during these optical studies. With increasing appreciation of their significance, we recorded the diameter and depth measurements of pits. These select measurements are summarized in Figure 34. Note that they generally group around L/D = 1, yet some features are significantly shallower, while others may be much deeper. It appears as if deeper pits occur preferentially on Tray 2 and very shallow structures on Tray 1, yet additional measurements are needed to evaluate whether this is indeed the case.

Residue Size and Flux Considerations

The size-distribution of projectile residue sizes is plotted in Figure 35. We need to emphasize that these particle-diameter measurements have substantial error, depending on absolute size, possibly as much as 50% for < 10 μm particles and ~ 20% for those > 20 μm. These uncertainties are related to dimensional measurements at the limit-of-resolution of the optical system employed, as well as to the difficulty in distinguishing between actual impactor residue and dense, molten aerogel material that envelopes many of these particles (*e.g.*, Barrett *et al.*, 1992). Also note the smaller number of measurements represented in Figure 34 compared to Figure 33, because many tracks did not contain measurable or visible residue at their termini. Nevertheless, note the grossly similar distributions for both trays, separated by 180° in viewing direction.

The particle-diameter measurements from both trays are plotted in cumulative fashion in Figure 36 and versus their cumulative frequency, the latter derived from the total cumulative exposure time (553 days) and surface area (0.106 m^2/tray analyzed optically). For comparison, we plot the LDEF derived mass distributions of small impactors, combining interplanetary dust and man-made debris (*e.g.*, Humes, 1991 and See *et al.*, 1993). Surprisingly, the general shape of these size distributions is fairly similar, and the flux values agree within an order of magnitude. As expected, the ODC particles < 10 μm are much more numerous than those derived from LDEF, due to significant comminution and ablative mass reduction of the ODC residues. In detail, we do not have a good explanation for the relatively steep curve segments at 10 - 25 μm diameter in both ODC distributions, but it is not an effect related to changes in optical resolution, as all scans were conducted at a constant magnification. Within statistical error, the fluxes on Trays 1 and 2 are essentially identical for particles > 15 μm, yet Tray 2 has a much higher flux at < 10 μm sizes, most likely attributable to the large number of small swarm particles.

Track Length versus Projectile Residue

The interpretation of microcraters in infinite half-space targets, such as on LDEF, is based on laboratory studies that reveal a systematic relationship between crater diameter and the initial impactor size/mass at any given projectile velocity (*e.g.*, Watts and Atkinson, 1992). Typically, any space-produced crater population is converted to a projectile-mass distribution by assuming a constant impactor density, as well as some mean encounter velocity. Unfortunately, the lack of reliable laboratory calibration experiments with aerogel (see Hörz *et al.*, 1997) does not permit

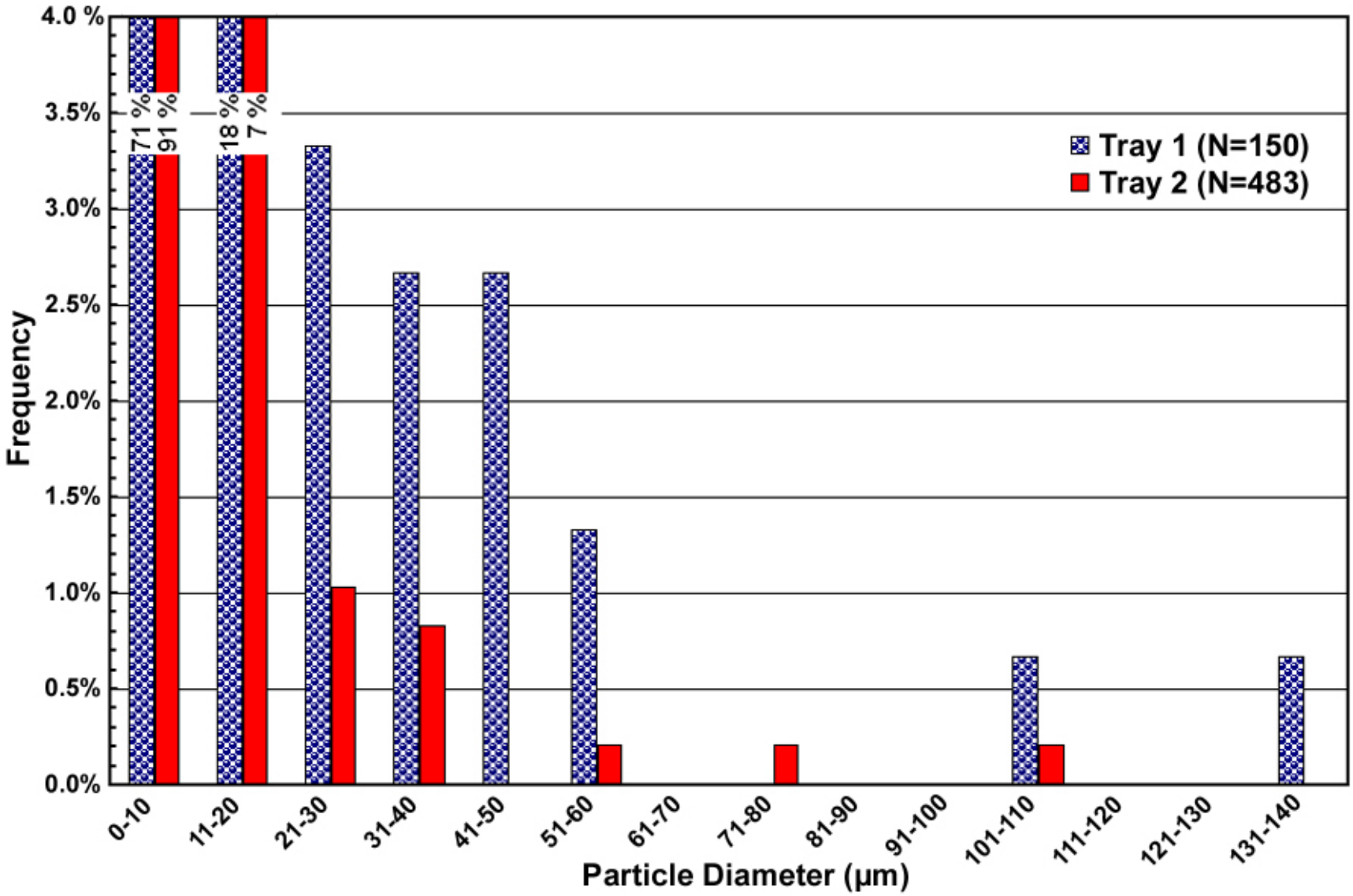

Figure 35. The distribution of projectile residue sizes based on in-situ measurements in unprocessed aerogel collectors using optical microscopy. These measurements may be afflicted with substantial errors, as it is difficult to optically recognize the extent of molten aerogel adhering to, or invading the projectile materials. The population is dominated by particles < 10 µm, close to the limit of the microscope's optical resolution.

such an approach for ODC. However, it may be very instructive to plot the observed residue size versus total track length to empirically explore whether some systematic relationship exists. Figure 37 illustrates the results, characterized by wide scatter. Tracks ranging in length from 1000 - 3000 µm are associated with residues that vary by an order of magnitude in size, and by some three orders of magnitude in mass. Conversely, tracks of widely divergent lengths may possess similar sized, small residues. In particular, most of the longer tracks are associated with relatively small particles, presumably due to ablative or abrasive mass loss of an initially much larger impactor. In addition, note that the largest residues in Figure 37 are associated with tracks that are not unusually long. We conclude that there is no systematic relationship between the size of the particle residue and the length of the associated track for the ODC aerogel. Similar

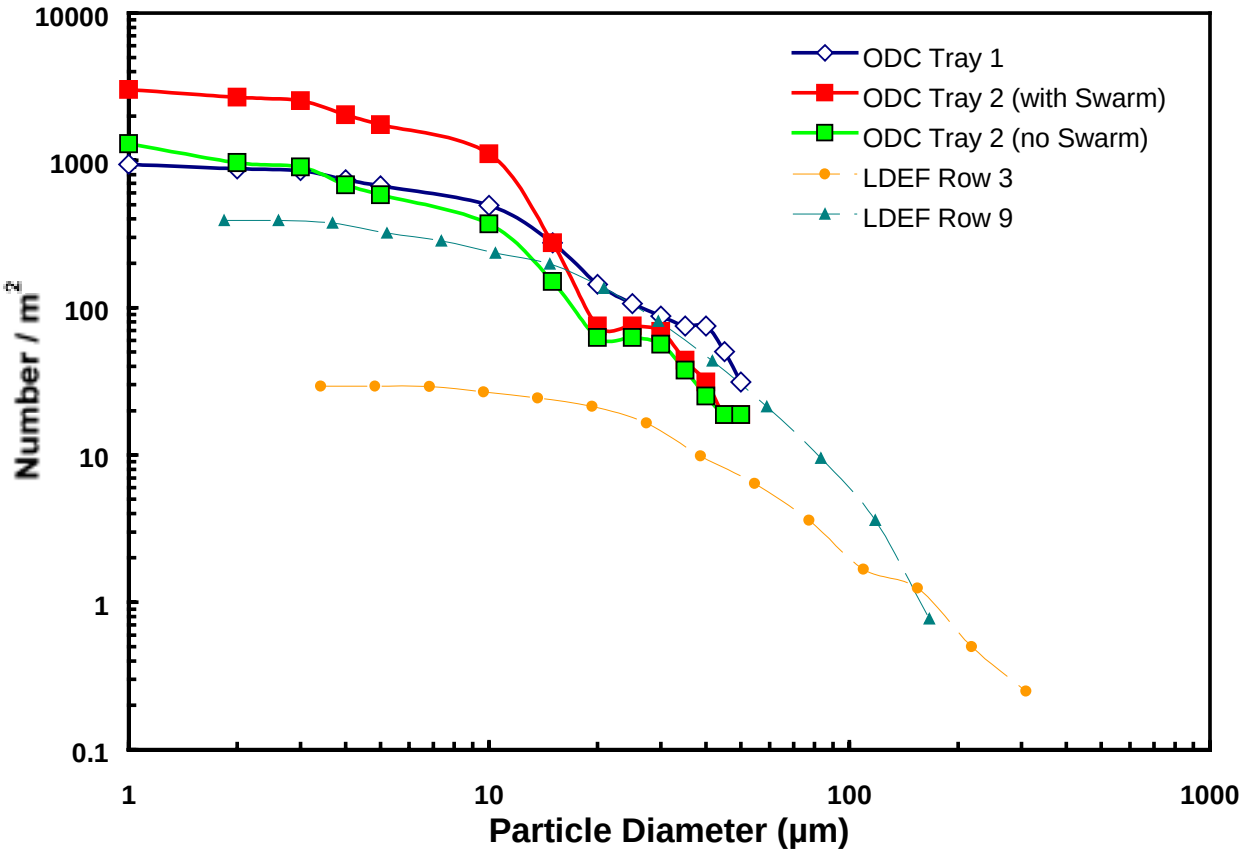

Figure 36. Cumulative particle fluxes in the ODC aerogel and comparison with LDEF data. The ODC data refers to direct measurements of (minimum) particle size. In contrast, the LDEF particle sizes are calculated from microcrater diameters in aluminum targets assuming some idealized impact conditions and using the equations of Wattsand Atkinson. (1993). Note the general agreement between ODC Tray 1 and Tray 2 (after subtraction of the swarm event; see Figures 40b for the quantitative identification of swarm tracks). In addition, note that Row 9 of LDEF occupied the leading edge, thus representing a maximum particle flux, while Row 3 occupied the trailing edge yielding a minimum flux (*e.g.*, Zook, 1991). The ODC data are somewhat deficient at large sizes and overabundant at the small sizes, both phenomena consistent with mass loss during capture.

results were reported from laboratory experiments (*e.g.*, Burchell and Thompson, 1996; Hörz *et al.*, 1997), yet Hörz *et al.* detail that much of the experimental scatter may be due to poorly known impactor mass. The empirical relationships shown in Figure 37 represent a more meaningful test of the desire to extract initial impactor mass (and other dynamic data such as velocity) from space-exposed aerogel. The process(es) of penetration and mass loss in aerogel must be highly idiosyncratic on a particle-by-particle basis and depend on a large number of variables, such as the encounter velocity, physical, and chemical properties of the projectile, and/or preexisting micro-cracks. It does not seem possible to extract major, initial impact conditions and particle properties from the dimensional measurements of tracks and associated particle residues. Finally, note that the distributions of track length and residue sizes are similar for both trays, again suggesting that Trays 1 and 2 experienced particle environments consisting of impactors with similar velocity and physical properties.

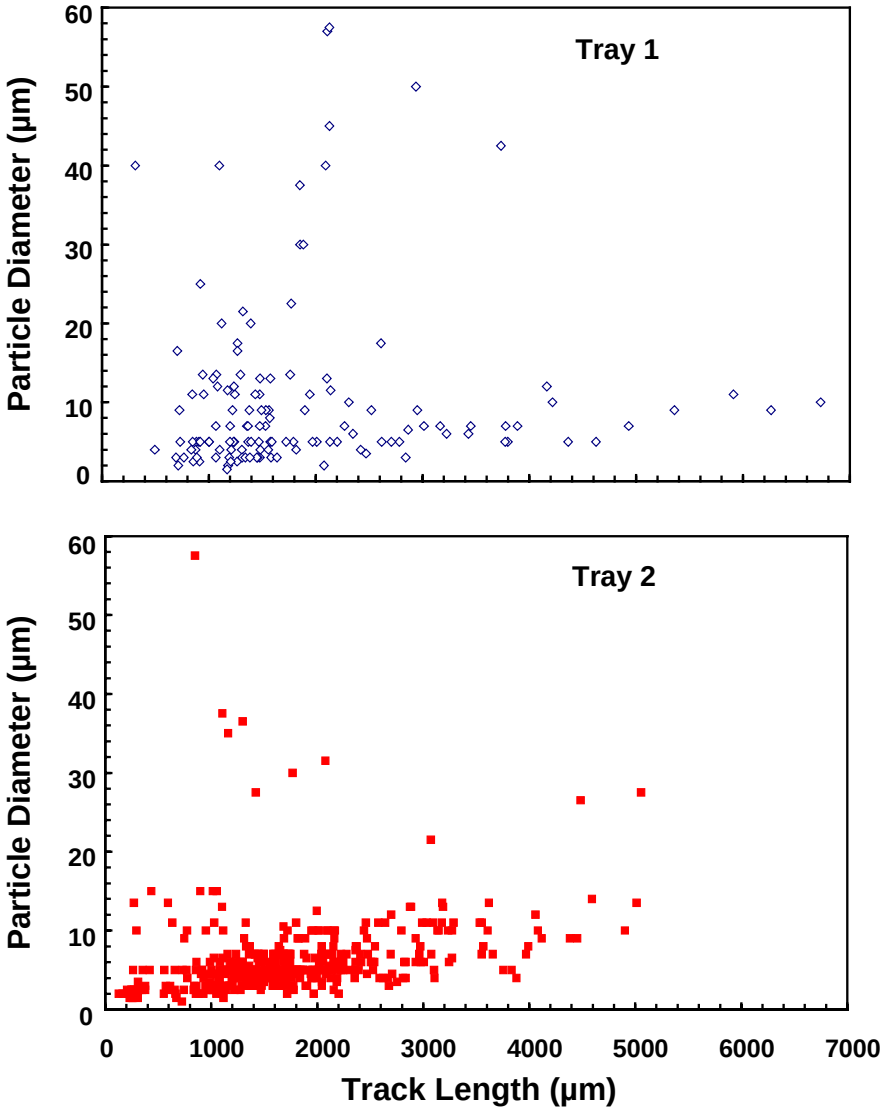

Figure 37. Track length versus diameter of the projectile residues for ODC Trays 1 and 2. The non-systematic relationship of residue mass and absolute track depth in aerogel seriously impairs the reconstruction of an initial impactor size and/or of encounter velocity (see text for detailed discussion).

Particle Trajectories

The trajectories of track-producing particles can be reconstructed from the measurements of X/Y/Z (entrance hole) and X'/Y'/Z' (end of track); the results of such calculations are illustrated in Figures 38 - 40. For a first-order impression we plotted track orientation from all tiles

projected on the area of a single tile in Figure 38. A directional vector of uniform length represents individual tracks, regardless of size, with the arrow pointing towards the terminus. The relatively random distribution on Tray 1 contrasts markedly with the highly lineated distribution of Tray 2, the latter data including tracks associated with the swarm event discussed earlier. The rose diagrams in Figure 39 present a more quantitative perspective. Tray 1 (Figure 39a) includes all tracks as portrayed in Figure 38 and suggests some modest, local maximum. Tray 2 (Figure 39b) is obviously so dominated by the swarm tracks that we subtracted all swarm tracks for a separate portrayal of the remianing population (Figure 39c).

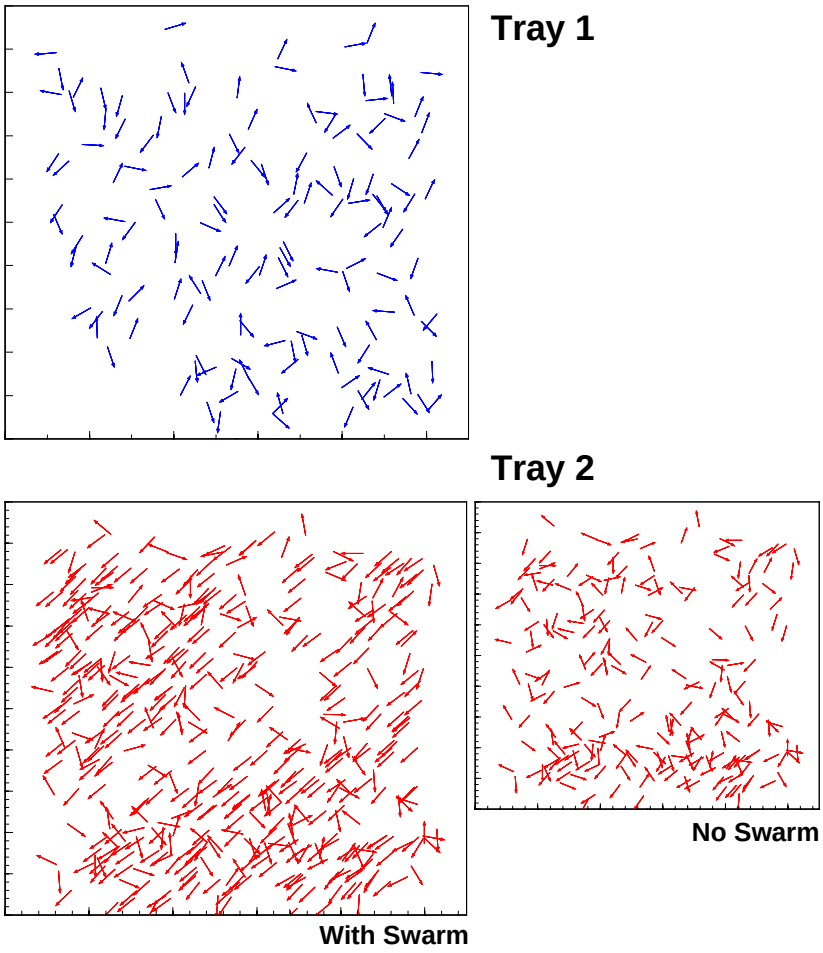

Figure 38. Azimuthal orientation of 148 tracks on ODC Tray 1 and of 435 tracks on Tray 2, the latter dominated by swarm particles of uniform direction (see text for details).

Finally, Figure 40 is a hemispherical (equal area) projection of measured track orientations that not only preserves the azimuth, but also the inclination of individual tracks; this portrayal reflects the true direction/radiant from which a particle approached ODC. A trajectory will *enter* the reference sphere surface at the plotted location (+), terminating at the center. For those not familiar with such plots, azimuthal relationships are as measured; the center of the plot represents vertical impacts (90°), the outer circle horizontal cases (0°), with intermediate inclinations linearly related to their radial distance from the center. Again, the trajectories of Tray 1 are generally random, with a modest maximum at approximately the 45° direction and of relatively shallow angles from the local horizontal. In contrast, Tray 2 is characterized by a pronounced maximum that represents the swarm tracks. The remaining tracks on Tray 2 are of fairly random orientations, similar to those of Tray 1. These similarities suggest either that there is no single dominant particle source from a specific radiant (excepting the secondary swarm event on Tray 2), or that the viewing directions of Mir/MEEP/ODC surfaces varied widely throughout the 553-day mission. In addition, one may also conclude that there was no local promontory that shielded large fractions of the field of view of either ODC tray.

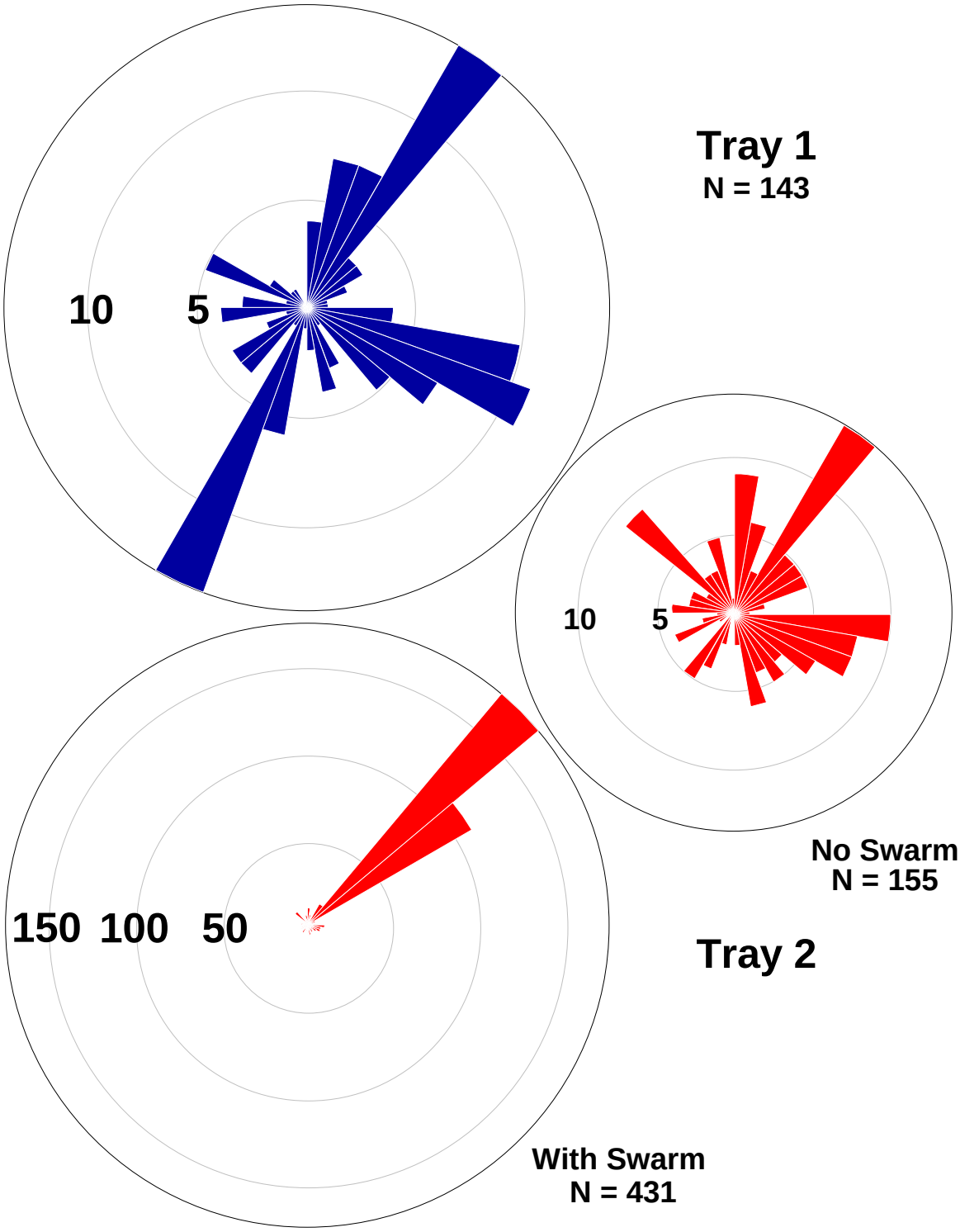

Figure 39. Rose diagram of aziumuthal track orientations for Tray 1 and Tray 2; Tray 2 is shown with and without (smaller inset) the swarm event. The sporadic populations on both trays display modest, local maxima.

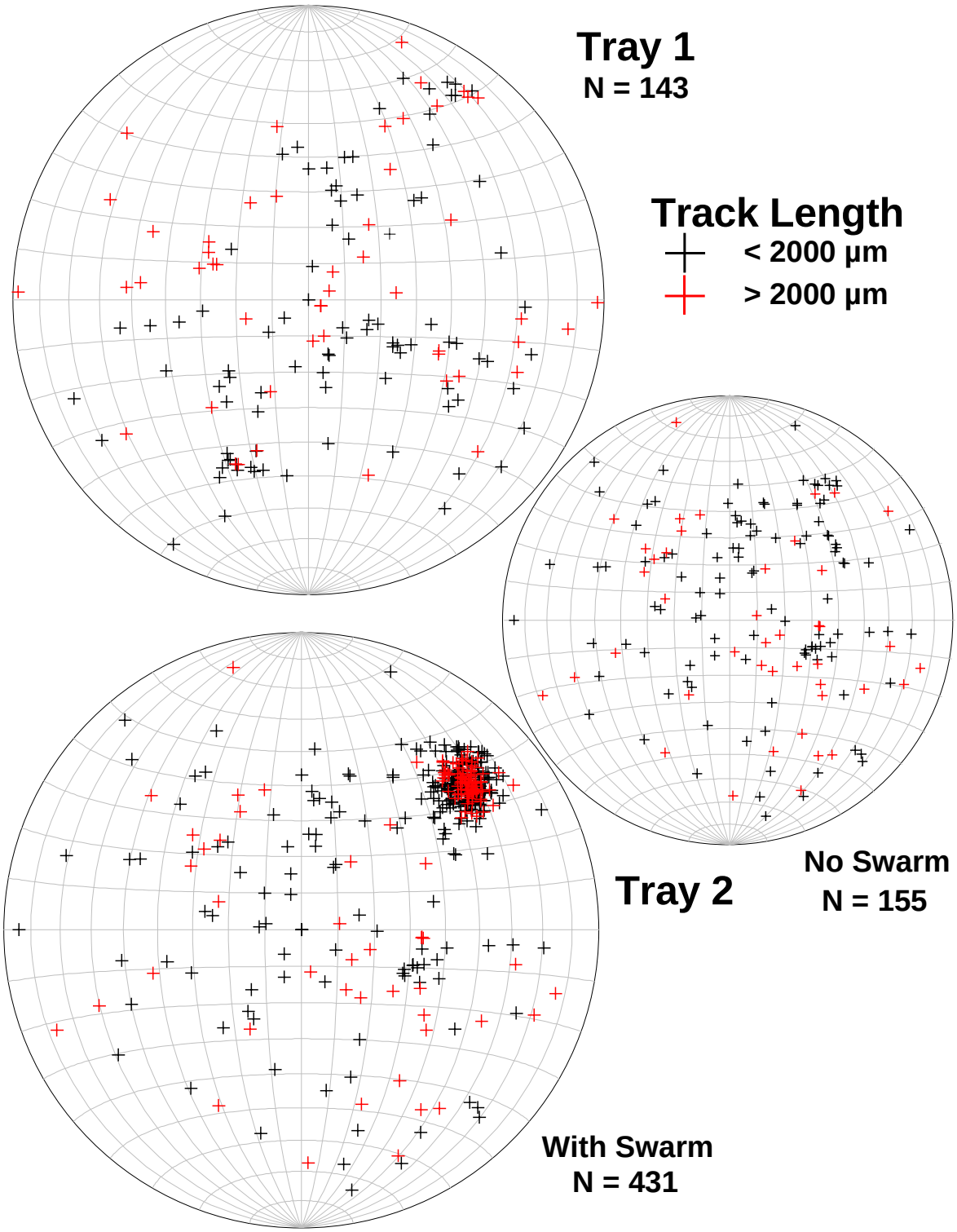

Figure 40. Quantitative illustration of track orientations utilizing an equal-area stereo projection. Again, Tray 2 is shown with and without the swarm events included. All tracks within 15° of the center of this cluster were assigned to the swarm event and subtracted from the measured population to yield the sporadic background of Tray 2 for all Figure 39 and 40s.